JOURNAL OF MATERIALS SCIENCE 25 (1990) 3338–3346

Synthesis of high-T_c superconducting Bi–Pb Sr–Ca–Cu–O ceramics prepared by an ultrastructure processing via the oxalate route

F. H. CHEN, H. S. KOO*, T. Y. TSENG
*Institute of Electronics, National Chiao Tung University, *and also Materials Research Laboratories, Industrial Technology Research Institute, Hsinchu, Taiwan*

The oxalate precursor yielded by a sol–gel processing can be pyrolysed and oxidized at 840° C for 40 h into the desired high-T_c superconductor in the lead-doped Bi–Sr–Ca–Cu–O system with $T_{c(onset)}$ = 140 K and $T_{c(zero)}$ = 104 K. The mechanisms of the sol–gel reaction were monitored by analysis of Fourier transformation infrared (FTIR) spectroscopy. Moreover, identification of the various phases existing on the specimens after firing at selected temperatures, was made by analysis by FTIR spectroscopy and X-ray diffractometry. Based on the experiment results, the mechanisms of forming $Bi_2Sr_2CaCu_2O_{8+\delta}$ (phase 2212) might be identified as the reaction of $Bi_2Sr_2CuO_{6+\delta}$, Ca_2CuO_3 and CuO at 800° C. Furthermore, $Bi_2Sr_2Ca_2Cu_3O_{10+\delta}$ (phase 2223) might be synthesized by the reaction of phase 2212, Ca_2CuO_3 and CuO at 840° C. Ca_2PbO_4 found in lead-doped materials may catalyse the formation reaction of Ca_2CuO_3 at 650° C and play a role of a flux to fuse $Bi_2Sr_2CaCu_2O_{8+\delta}$, CuO and residual Ca_2CuO_3 and then improve the further synthesis of $Bi_2Sr_2Ca_2Cu_3O_{10+\delta}$ at 840° C.

1. Introduction

Since a new superconducting material in the Bi–Sr–Ca–Cu–O system was discovered by Maeda *et al.* [1] with critical transition temperatures at about 80 and 110 K, a vast amount of research has been focused on how to stabilize or increase the bulk of the high-T_c phase which was identified as $Bi_2Sr_2Ca_2Cu_3O_{10+\delta}$ (phase 2223), being a tetragonal or pesudotetragonal structure with lattice parameters a = 0.539 nm and c = 3.71 nm. The so-called low-T_c phase was identified as $Bi_2Sr_2CaCu_2O_{8+\delta}$ (phase 2212) with lattice parameters a = 0.539 nm and c = 3.06 nm [2, 3]. So far, the addition of excess calcium and copper [4, 5], prolonging the sintering time [6], and a low oxygen partial pressure sintering process [7], have been used to increase the volume fraction of the high-T_c phase. Recently, Takano *et al.* [8] succeeded in stabilizing phase 2223 with $T_{c(onset)}$ = 105 K by partial substitution of lead for bismuth, using a coprecipitation method.

In this report, the superconductor $Bi_{0.8}Pb_{0.2}SrCaCu_2O_y$ was prepared by a sol–gel processing via the oxalate route. Compared to a traditional solid-state method, it is well known that the precursor derived from a sol–gel method, consisting of submicrometre-scale particles with excellent homogeneity, is able to be decomposed into desirable materials with high reproducibility and sinterability using a relatively low sintering temperature and shorter heat-treatment time. In addition, a sol–gel technology can be employed to the applications of shape forming (e.g. films and wires) and microceramics manipulation (e.g. coatings and fibres).

Such a sol–gel processing had been used to create the Y–Ba–Cu–O [9–13] and Bi–Sr–Ca–Cu–O [14] superconducting systems. The present work is aimed not only at preparing a high-reproducibility high-T_c superconductor in the Bi–Pb–Sr–Ca–Cu–O system, derived from the oxalate precursor, but also at studying the reaction mechanisms of lead-containing material before firing and after heat treatment at various temperatures, by the analyses of a Fourier transformation infrared (FTIR) spectroscopy and X-ray diffractometry.

2. Experimental procedure

2.1. Preparation of specimens

The superconducting oxide with a nominal composition $Bi_{0.8}Pb_{0.2}SrCaCu_2O_y$ was synthesized via the metal oxalate route using high-purity nitrate salts as starting materials: $Bi(NO_3)\cdot 5H_2O$, $Pb(NO_3)_2$, $Sr(NO_3)_2$, $Ca(NO_3)_2\cdot 4H_2O$ and $Cu(NO_3)_2\cdot 3H_2O$. The stoichiometric amount of each nitrate salt was added to an ethylene glycol solution of oxalic acid in the cationic ratio Bi : Pb : Sr : Ca : Cu = 0.8 : 0.2 : 1 : 1 : 2, followed by vigorous stirring. The oxalate gel was formed by the reaction of stoichiometric metal nitrates with the ethylene glycol solution of oxalic acid. In order to ensure the presence of sufficient oxalic acid anions, such as $HC_2O_4^{-1}$ and $C_2O_4^{-2}$, to bind the metal cations, excess oxalic acid was used. Ammonium hydroxide (15.35 N) was then used to adjust the pH of the above solution. Subsequently, the resulting solution after ageing, drying and grinding treatments, was transformed into a solid precursor. The precursor was then calcined at 800° C for 6 h. After regrinding and

0022–2461/90 $03.00 + .12

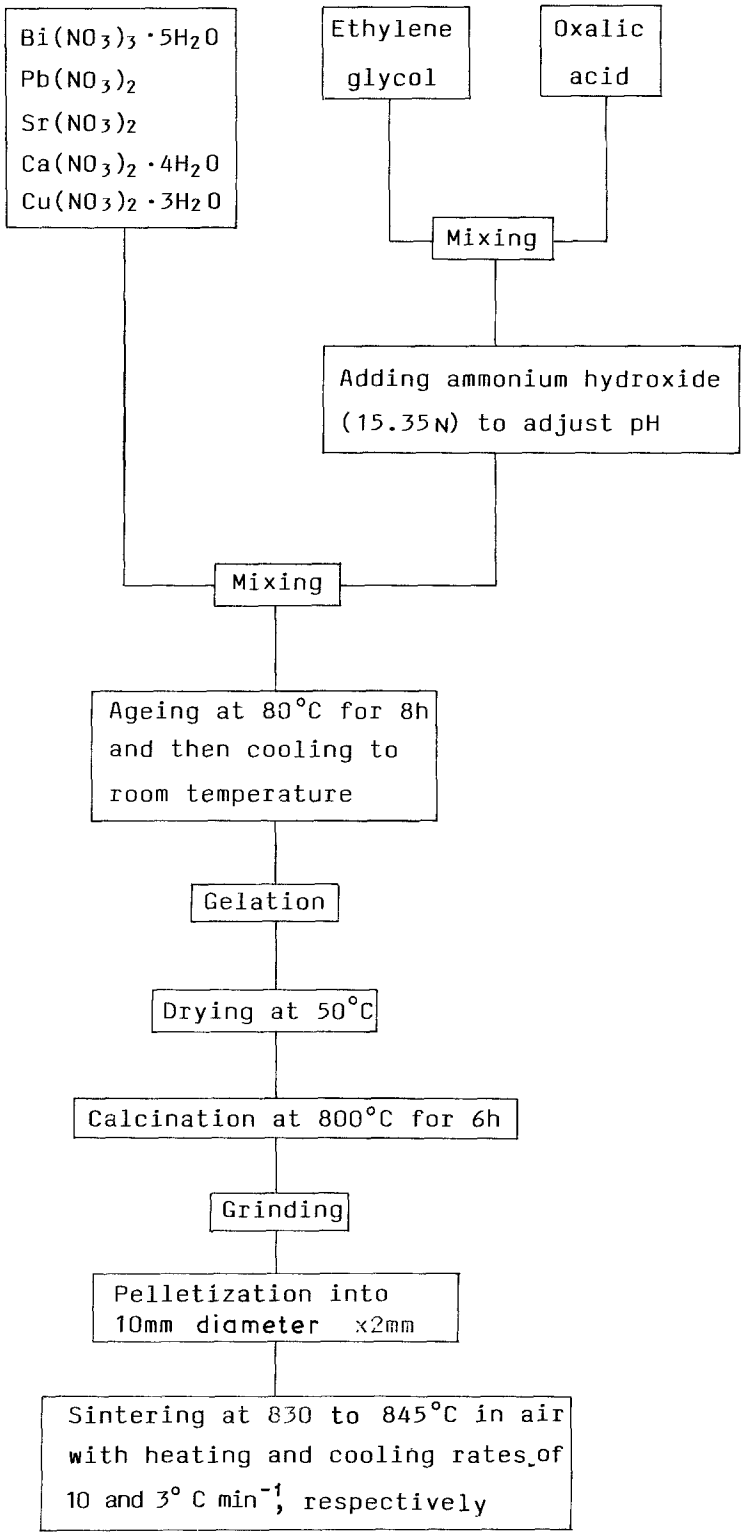

Figure 1 Schematic diagram of the preparation of the superconductor in the Bi–Pb–Sr–Ca–Cu–O system via the oxalate route.

pelletization, the calcination material was finally sintered at 840 to 845° C for various times, followed by cooling to room temperature at a rate of 3° C min^{-1}. A schematic diagram of the preparation of the specimens is shown in Fig. 1.

2.2. Characterization of reaction mechanisms

Fourier transformation infrared (FTIR) spectroscopy was used to study the mechanisms of the sol–gel reaction to form a gel-like oxalate and the phase transformation of powders after firing at various temperatures. The identification of various phases existing in the precursor, calcined and sintered specimens was carried out by X-ray diffraction analysis with 2θ in the range from 3° to 65° using Cu$K\alpha$ radiation in a Philips diffractometer. Thermogravimetric analysis (TGA) and differential thermal analysis (DTA) at a heating rate of 10° C min^{-1} in static air were employed to assist in understanding the reactions of pyrolysis of the precursor on heating.

2.3. Study of electrical properties and microstructures

The temperature dependence of electrical resistance of the sintered specimen was measured by the standard four-probe method. The bright-field images of sol, as-gelled sample, as-dried precursor, calcined and sintered samples were obtained using a Hitachi H-600

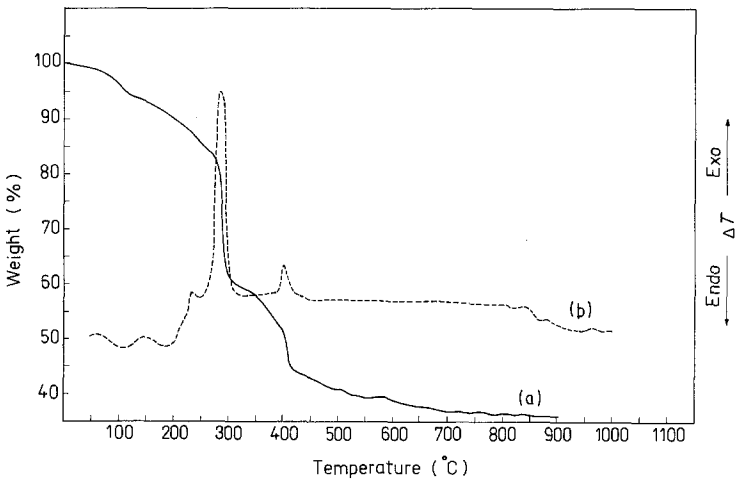

Figure 2 Data of (a) thermogravimetric analysis and (b) differential thermal analysis of the oxalate precursor at a heating rate of 10° C min^{-1}.

transmission electron microscopy (TEM) at 75 kV. The fracture surface of the sintered specimen was observed using a Hitachi S-570 scanning electron microscopy (SEM) performing at 20 kV.

3. Results and discussion

3.1. Thermal data of the oxalate precursor

Fig. 2 curve (a) shows thermograms of the oxalate precursor which displays a gradual weight loss from 100 to 280° C. Two abrupt losses were seen at about 280 and 400° C. This result indicates that the precursor was decomposed in two distinct steps. The first step is associated with the losses of organic moieties and the decomposition of partial metal oxalates. The second step is due to the pyrolysis of residual metal oxalates into carbonates and oxides. A similar study in the Y–Ba–Cu–O system derived from a citrate precursor was reported by Sale and Mahloojchi [15]. The DTA data of the precursor are shown in Fig. 2 curve (b). Two sharp exothermic peaks, corresponding to the two-step weight losses exhibited in Fig. 2a, are indicative of the evolution of many gases and much heat resulting from the decomposition of the precursor at 280 and 400° C. Two weaker endothermic peaks at about 820 and 870° C indicate the partial melting of the resulting material.

3.2. Characterization of samples

Fig. 3 shows the FTIR spectra of the oxalate precursor and its products after decomposition at selected temperatures. The spectrum of the as-dried precursor is shown in Fig. 3a with characteristic frequencies (cm^{-1}) at 490 (M–O, O–M–O, M = metal components; O = oxides), 781 (C–O–M), 1418 (doublet C–C in ethylene glycol) and 1643–1647 caused by the vibration of the C=O bond in metal oxalate complexes. The possible sol–gel reactions corresponding to dissociation, recombination, hydrolysis, polymerization and complex formation in this nitrate–oxalate solution system are shown below.

(I) Dissociation

$$M(NO_3)_n \cdot xH_2O \rightarrow M^{n+} + nNO_3^{-1} + xH_2O$$

$$n = 2, 3$$

$$HO(CH_2)_2O\text{–}H + OH^- \rightarrow HO(CH_2)_2O^- + H_2O$$

↑ coming from the dissociation of NH_4OH.

(II) Recombination

$$M^{2+} + 2HO(CH_2)_2O^- \rightarrow HO(CH_2)_2O\text{–}M\text{–}O(CH_2)OH$$

(III) Hydrolysis

$$HO(CH_2)_2O\text{–}M\text{–}O(CH_2)_2OH + H\text{–}O\text{–}H \rightarrow HO(CH_2)_2O\text{–}M\text{–}O\text{–}H + HO(CH_2)_2OH$$

(IV) Polymerization

$$HO(CH_2)_2O\text{–}M\text{–}O(CH_2)_2OH + H\text{–}O\text{–}M\text{–}O(CH_2)_2OH \rightarrow HO(CH_2)_2O\text{–}M\text{–}O\text{–}M\text{–}O(CH_2)_2OH + HO(CH_2)_2OH$$

(V) Complexation

$$M^{n+} + xHC_2O_4^- \rightarrow M(HC_2O_4)_x^{n-x} \quad n = 2, 3$$

$$M^{n+} + xC_2O_4^{2-} \rightarrow M(C_2O_4)_x^{n-2x} \quad n = 2,3$$

$$HO(CH_2)_2O\text{–}M\text{–}OH + HC_2O_4^- \rightarrow HO(CH_2)_2O\text{–}M\text{–}OH_2^+C_2O_4^{2-}$$

In order to simplify the above equations, only the divalent metal ions M^{2+} (e.g. Pb^{2+}, Sr^{2+}, Ca^{2+} and Cu^{2+}) instead of trivalent metal ions M^{3+} (e.g. Bi^{3+}) were investigated in recombination, hydrolysis and polymerization. The addition of ammonium hydroxide to the ethylene glycol solution of oxalic acid has both of functions of pH adjustment and improving the reaction rate of dissociation. On the other hand, the peaks corresponding to $CaC_2O_4 \cdot H_2O$ were also found in Fig. 3a at 1318 and 780 cm^{-1}.

The IR spectrum of the calcination sample at 300° C for 3 h is shown in Fig. 3b with typical $CaCO_3$, $SrCO_3$ and CuO absorption peaks at 875, 857 and 605 cm^{-1}, respectively, accompanied by the disappearance of 1318 and 780 cm^{-1}. When the sample was fired at 650° C for 3 h, the characteristic 875 cm^{-1} frequency disappeared. Subsequently, only the stretching of CuO was found at 606 cm^{-1} in the sample calcined at 800° C for 6 h, indicating complete decomposition of carbonates at this stage.

The phase identification for the as-dried precursor, calcined powders and sintered pellets by X-ray diffraction analysis is given in Table I. The products of the

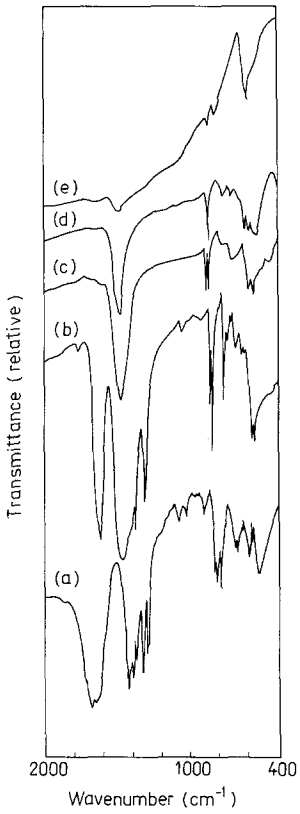

Figure 3 Fourier transformation infrared spectra of (a) the oxalate precursor, and the resulting materials after firing at (b) 300° C, (c) 500° C (d) 650° C for 3 h, and (e) 800° C for 6 h.

precursor after drying at 50° C are calcium and copper hydrates, which is indicative of the complexity of the sol–gel reation. Such a reaction is strongly influenced by pH, concentration of the starting materials and ageing temperature. For example, the influence of pH on the formation constants of barium citrate complexes was reported previously [11]. Brinker and Scherer [16] reported that the stability of a "frozen-in" structure caused by the polymerization of hydrolysed metal alkoxides in an alcoholic solution is dependent on the range of temperature, water content and pH. In addition, Tseng *et al.* [17] also proposed that an MgO–PSZ gel produced under higher NH_4OH concentration favours an assembly of linear or planar polymerized particles which have a larger pore volume and pore size.

After heating to 300° C, the metal oxalates were decomposed into calcium and strontium carbonates together with copper oxide. When a sample was fired at 650° C for 3 h, Ca_2PbO_4, Ca_2CuO_3 and $Bi_2Sr_2CuO_{6+\delta}$ were detected. $Bi_2Sr_2CuO_{6+\delta}$ was discovered with a critical transition temperature of only 7 K [18, 19]. Kijima *et al.* [20] and Uzumaki *et al.* [21] studied the roles of Ca_2PbO_4 and $Bi_2Sr_2CuO_{6+\delta}$ in the Bi–Pb–Sr–Ca–Cu–O system and suggested that the high-T_c phase, which is caused by the reaction between the low-T_c structure and Ca^{2+} in the liquid phase, is caused by the decomposition of Ca_2PbO_4 at 822° C. As the sample was calcined at 800° C for 3 h, $Bi_2Sr_2CaCu_2O_{8+\delta}$ was formed and $Bi_2Sr_2CuO_{6+\delta}$ decayed after firing for 6 h. It is clear that the phases by FTIR spectra of specimens after calcination at 300, 500, 650 and 800° C are in accordance with those determined by XRD analysis. After sintering at 840° C for 16 h, phase 2223 was formed. When the sintering was prolonged to 40 h, Ca_2CuO_3 disappeared, accompanied by a decrease in CuO and phase 2212, but an increase in phase 2223. The corresponding X-ray diffraction patterns of materials calcined at 650 and 800° C and sintered at 840° C are shown in Fig. 4. The above results may be explained by the following reaction mechanisms.

(I) At 650° C

$$CaCO_3 \rightarrow CaO + CO_2\,(g)\uparrow \quad (1)$$

$$2CaO + CuO \rightarrow Ca_2CuO_3 \quad (2)$$

(II) At 800° C

$$2Bi_2Sr_2CuO_{6+\delta} + Ca_2CuO_3 + CuO \rightarrow 2Bi_2Sr_2CaCu_2O_{8+\delta} \quad (3)$$

(III) At 840° C

$$2Bi_2Sr_2CaCu_2O_{6+\delta} + Ca_2CuO_3 + CuO \rightarrow 2Bi_2Sr_2Ca_2Cu_3O_{10+\delta} \quad (4)$$

In order to make a comparison, the XRD pattern of lead-free material after calcining at 720° C for 5 h is shown in Fig. 4f. We found that the peak intensity of Ca_2CuO_3 in lead-free material is much weaker than that in lead-doped material calcined at 650° C for 3 h. Ca_2PbO_4 may be thought of as a catalyst of Reaction 2, that is, Ca_2PbO_4 may accelerate the formation reaction of Ca_2CuO_3 and decrease the formation temperature. When the heat-treatment temperature is 840° C, Ca_2PbO_4 melts (m.p. = 822° C [22]), which corresponds to the small endothermic peak at 820° C seen in Fig. 2b, and may play the role of a flux to fuse $Bi_2Sr_2CaCu_2O_{8+\delta}$, CuO and residual Ca_2CuO_3 and then improve the further synthesis of $Bi_2Sr_2Ca_2Cu_3O_{10+\delta}$. Although no attempts were made in Equations 3 and 4 to consider the substitution behaviour of lead for bismuth atoms, it is ensured that a partial substitution of lead for bismuth will result in changing the original structures of phases 2212 and 2223 [23]. Basically, we do

TABLE I Phase determined by XRD in heat-treated samples

Heat-treatment conditions (° C) (h)	Phases
50 × 8	$CuC_2O_4 \cdot xH_2O$, $CaC_2O_4 \cdot H_2O$
300 × 3	CuO, $CaCO_3$, $SrCO_3$
500 × 3	CuO, Bi_2O_3, $SrCO_3$, $CaCO_3$
650 × 3	CuO, Bi_2O_3, $CaCO_3$, $SrCO_3$, SrO, Ca_2PbO_4, Ca_2CuO_3, $Bi_2Sr_2CuO_{6+\delta}$
800 × 3	CuO, Ca_2PbO_4, Ca_2CuO_3, $Bi_2Sr_2Cu_{6+\delta}$, $Bi_2Sr_2CaCu_2O_{8+\delta}$
800 × 6	CuO, Ca_2PbO_4, Ca_2CuO_3, $Bi_2Sr_2CuO_{6+\delta}$(trace), $Bi_2Sr_2CaCu_2O_{8+\delta}$
840 × 16	CuO, Ca_2PbO_4, Ca_2CuO_3, $Bi_2Sr_2CuO_{6+\delta}$(trace), $Bi_2Sr_2CaCu_2O_{8+\delta}$, $Bi_2Sr_2Ca_2Cu_3O_{10+\delta}$
840 × 40	CuO, Ca_2PbO_4(trace), $Bi_2Sr_2CaCu_2O_{8+\delta}$, $Bi_2Sr_2Ca_2Cu_3O_{10+\delta}$

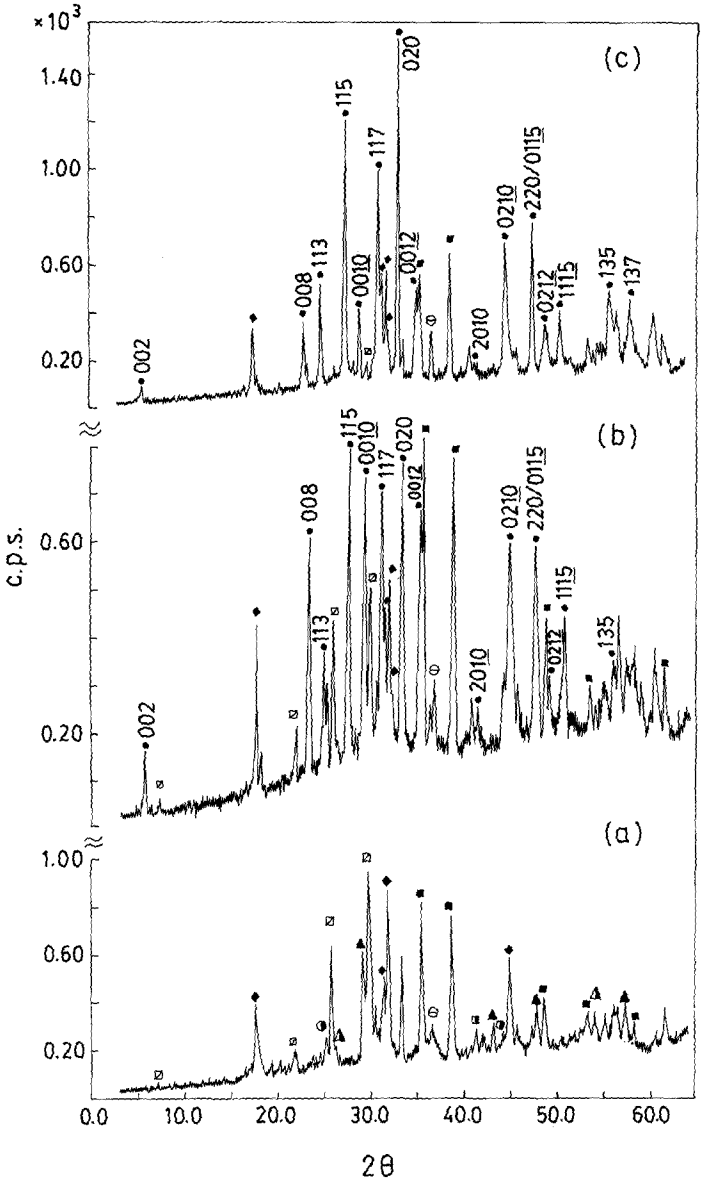

Figure 4 X-ray diffraction patterns for the lead-doped powders calcined at (a) 650° C for 3 h, (b) 800° C for 3 h, (c) 800° C for 6 h, and sintered at (d) 840° C for 16 h, (e) 840° C for 40 h, and the lead-free material (f) calcined at 720° C for 5 h. The indices (hkl) with no markings belong to phase 2223. (■) CuO, (◨) SrO, (◆) Ca_2PbO_4, (⧄) $Bi_2Sr_2CuO_{6+\delta}$, (◑) $SrCO_3$, (▲) Bi_2O_3, (▲) $CaCO_3$, (⊖) Ca_2CuO_3, (●) phase 2212.

not exclude the probability that the partial substitution of lead for bismuth in BiO layers will create the vacancies in oxygen sites. The cluster of vacancies may reduce the energy barrier for the insertion of calcium and CuO_2 sheets into $Bi_2Sr_2CuO_{6+\delta}$ to form the 2212 phase or into $Bi_2Sr_2CaCu_2O_{8+\delta}$ to form the 2223 phase if the heat-treatment time was prolonged, reconciling the fact that the stabilization of phase 2223 by the addition of lead is a slow kinetic process.

Little work has been reported to explain the reaction mechanisms for the formation of the high-T_c phase in the Bi–Pb–Sr–Ca–Cu–O system which was prepared by solid-state reaction. Kijima *et al.* [20] reported that the high-T_c phase and $Bi_2Sr_2CuO_x$ were obtained from the disproportionate reaction of the low-T_c phase, and Uzumaki *et al.* [21] reported that a high-T_c phase was synthesized by adding Ca_2PbO_4 to the Bi–Sr–Cu–O system. Nevertheless, the XRD data in the present paper indicate that $Bi_2Sr_2CuO_{6+\delta}$ formed at 650° C was not accompanied by the existence of either phase 2212 or 2223 and $Bi_2Sr_2CuO_{6+\delta}$ almost vanished after the sample was calcined at 800° C for 6 h without the formation of phase 2223. These diverse phase transition sequences compared to the previous results [20, 21] may be caused by the different preparation processes, which induce variable kinetics, in the samples.

Fig. 5 shows bright-field transmission electron micrographs of the sol, as-gelled sample, as-dried precursor, calcination and sintering samples. Typical networks were found in Figs 5a and b. The size of the ultrastructure of the as-gelled sample is larger than that of the sol. These phenomena powerfully confirm the occurrence of a polymerization mechanism in the sol–gel reaction. Although the oxalate precursor in the present work consists of a trace of crystalline phase detected by XRD and FTIR analyses, a very homogeneous solution of starting materials, mixed by molecular-dimension or nearly molecular-dimension manipulation, can be anticipated. The particle size of the as-dried precursor shown in Fig. 5c, lay in the range 100 to 200 nm, which ascertains that it has a relatively large specific surface area and results in a high sinterability during subsequent heat treatment. The morphologies of irregular particles of samples fired at various temperatures can be clearly observed in Figs. 5d to f. The higher the calcination temperature, the larger is the particle size of lead-doped material, which has simultaneously a clearer-cut surface. As shown in Figs 5e and f, plate-like particles can

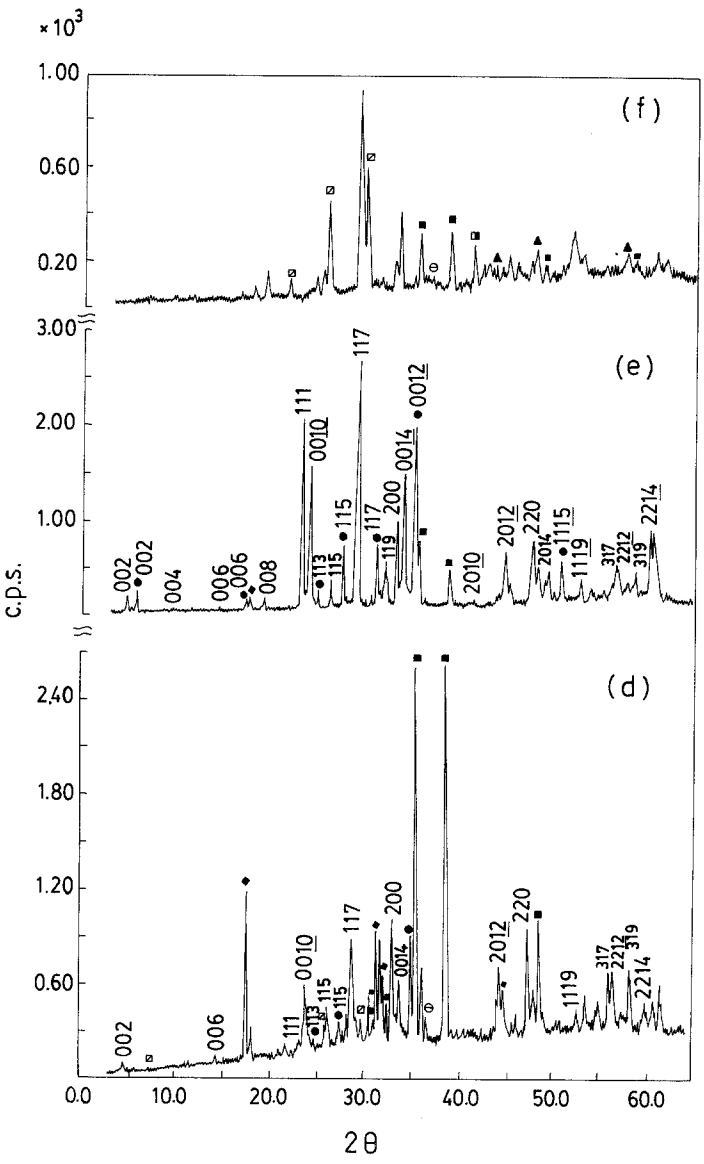

Figure 4 Continued.

be found in those samples calcined at 800° C for 6 h and sintered at 840° C for 40 h, respectively.

3.3. Characterization of sintered materials

Fig. 6 demonstrates the characteristics of the temperature dependence of electrical resistance for $Bi_{0.8}Pb_{0.2}SrCaCu_2O_y$ bulk specimens sintered at 840° C for 16 h (sample A) and 40 h (sample B). The onset temperature of both samples is at about 140 K. The more probable explanation for the very high $T_{c(onset)}$ may be that the sample, prepared by a sol–gel method, has excellent homogeneity and sinterability. A similar result was reported by Sastry *et al.* [24] who prepared $Bi_{1.6}Pb_{0.4}Ca_2Sr_2Cu_3O_y$ with $T_{c(onset)} = 140$ K and $T_{c(zero)} = 120$ K, using a precursor–matrix solid-state reaction method together with partial melting, long-term sintering and several intermediate grinding treatments. Sample B shows an end critical temperature of 104 K, but a tail of resistance makes the $T_{c(zero)}$ of sample A drop to 90 K. It suggests that treatment by prolonging the sintering time in the Bi–Pb–Sr–Ca–Cu–O system is more effective in stabilizing the 2223 phase. In other words, the reaction such as Equation 4 will be capable of progressing more completely as long as the sintering time is prolongated. It is notable that the crystallization time and temperature necessary to obtain the desired superconductors created by a sol–gel processing, are less than those employed for the conventional solid-state reaction method. Fig. 7 shows scanning electron micrographs of the fracture surfaces of specimens sintered at 840° C for 5, 16 and 40 h. It can be seen that in all samples, lamellar plate-like grains were found, which were described as a sequence of 2212 and 2223 layers [25]. In addition, grains being well crystallized in a sample sintered at 840° C for only 5 h is further powerful proof that the oxalate precursor has a high sinterability.

4. Conclusions

1. The high-T_c superconducting oxide in the Bi–Pb–Sr–Ca–Cu–O system can be synthesized with $T_{c(onset)} = 140$ K and $T_{c(zero)} = 104$ K by a sol–gel processing via the oxalate route. Compared to the conventional solid-state reaction method, the precursor derived from an oxalate gel, which was confirmed by TEM bright image to have a particle size of 100 to 200 nm, possesses a high sinterability, and results in a relatively low sintering temperature and a faster rate of transformation from phase 2212 to 2223.

2. The mechanisms of the sol–gel reaction monitored using FTIR spectroscopy analysis include dissociation, recombination, hydrolysis, polymerization

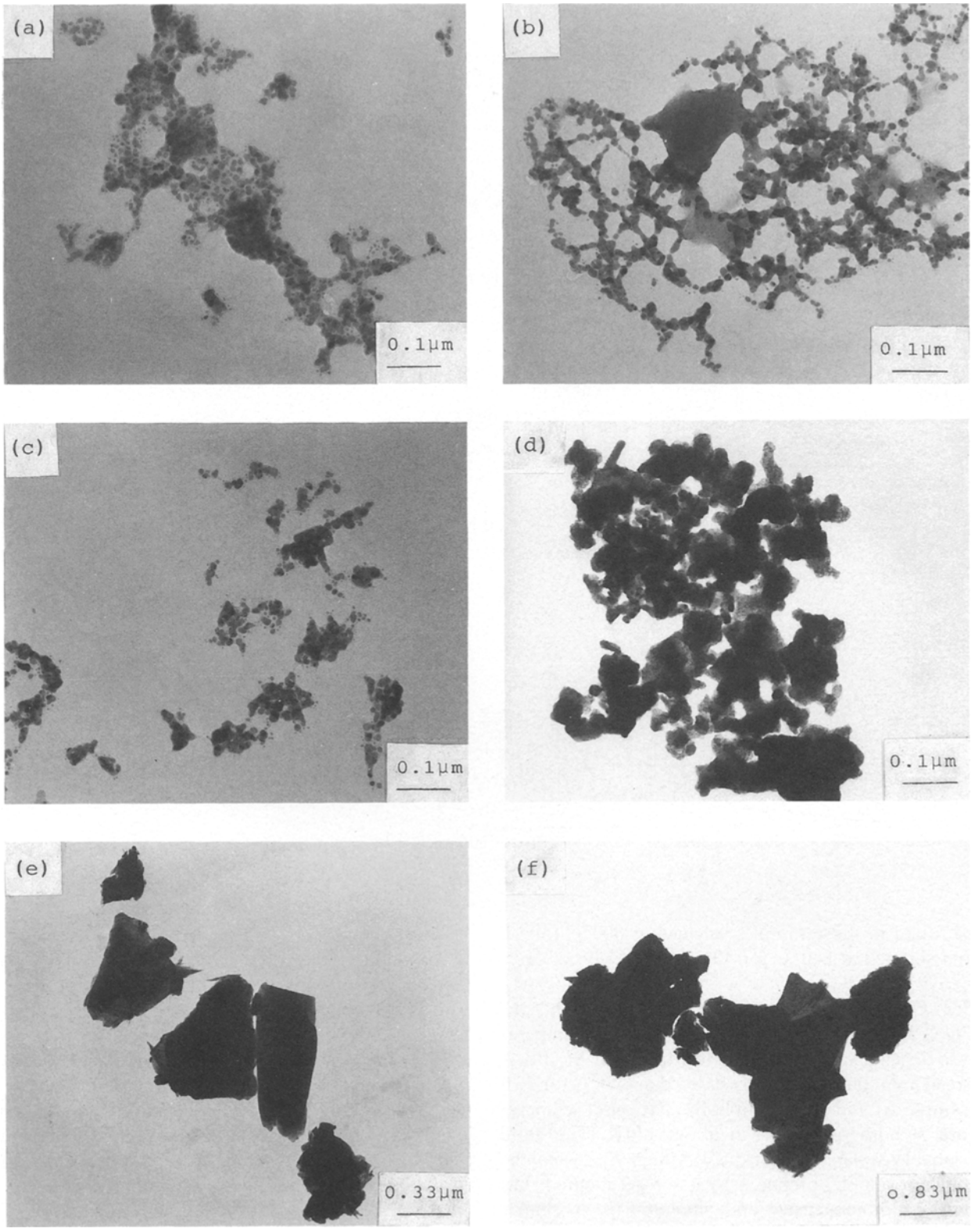

Figure 5 Transmission electron micrographs of (a) sol, (b) as-formed gel, (c) as-dried precursor, the samples (d) calcined at 500° C for 3 h, (e) calcined at 800° C for 3 h, and (f) sintered at 840° C for 40 h.

and complex formation. Changes in the FTIR spectra of the resulting materials decomposed at 300, 500, 650 and 800° C are in agreement with those determined by XRD analysis.

3. The mechanisms of forming $Bi_2Sr_2CaCu_2O_{8+\delta}$ phase might be identified as the reaction of $Bi_2Sr_2CuO_{6+\delta}$, Cu_2CuO_3 and CuO at 800° C. $Bi_2Sr_2Ca_2Cu_3O_{10+8}$ might be the synthesized by the reaction of $Bi_2Sr_2CaCu_2O_{8+\delta}$, Ca_2CuO_3 and CuO at 840° C. Ca_2PbO_4 in lead-doped material may catalyse the formation of Ca_2CuO_3 at 650° C and play a role of a flux to fuse $Bi_2Sr_2CaCu_2O_{8+\delta}$, CuO and residual Ca_2CuO_3 and then improve further synthesis of $Bi_2Sr_2Ca_2Cu_3O_{10+\delta}$.

4. The pyrolysis data of the as-dried oxalate precursor indicated that the precursor was decomposed in two distinct steps: one occurring at about 280° C associated with the loss of the organic moieties and decomposition of the partial metal oxalates; the other at about 400° C corresponds to the pyrolysis of residual oxalates.

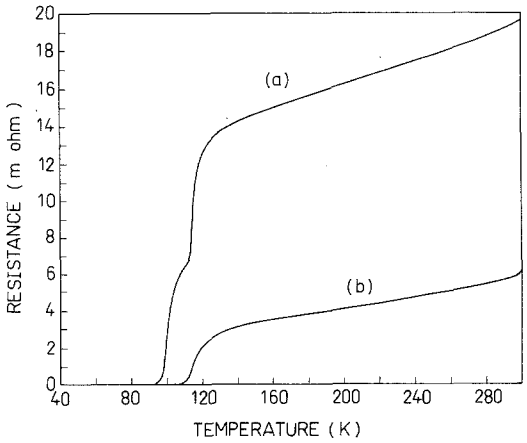

Figure 6 The characteristics of temperature dependence of electrical resistance of $Bi_{0.8}Pb_{0.2}SrCaCu_2O_y$ sintered at 840° C for (a) 16 h and (b) 40 h.

5. Alternating layers of 2212 and 2223 phases indicated by the lamellar plate-like grains were found in $Bi_{0.8}Pb_{0.2}SrCaCu_2O_y$ sintered at 840° C only for 5 h, further proof that the oxalate precursor has a high sinterability.

Acknowledgement

The authors thank Mr Y. S. Fran for his help with Fourier transformation infrared spectroscopy and for useful suggestions.

References

1. H. MAEDA, Y. TANAKA, M. FUKUTOIMI and T. ASANO, *Jpn J. Appl. Phys.* **27** (1988) L209.
2. E. TAKAYAMA-MUROMACHI, Y. UCHIDA, A. ONO, F. IZUMI, M. ONODA, Y. MATSUI, K. KOSUDA, S. TAKEKAWA and K. KATO, *ibid.* **27** (1988) L365.
3. J. M. TARASCON, W. R. MCKINNON, P. BARBONX, D. M. HWANG, B. G. BAGLEY, L. H. GREENE, G. W. HULL, Y. LePAGE, N. STOFFEL and M. GIROUND, *Phys. Rev. B* **38** (1988) 8885.
4. A. SUMIYAMA, T. YOSHITOSHI, H. ENDO, J. TSUCHIYA, N. KIJIMA, M. MIZUNO and Y. OGURI, *Jpn J. Appl. Phys.* **27** (1988) L542.
5. N. KIJIMA, H. ENDO, J. TSUCHIYA, A. SUMIYAMA, M. MIZUNO and Y. OGURI, *ibid.* **27** (1988) L821.
6. H. NOBUMASA, K. SHIMIZU, Y. KITANO and T. KAWAI, *ibid.* **27** (1988) L846.
7. K. KITAZAWA, S. YAEGASHI, K. KISHIO, T. HASEGAWA, K. PARK and K. FUEKI, *Adv. Ceram. Mater.*
8. M. TAKANO, J. TAKADA, K. ODA, H. KITAGUCHI, Y. IKEDA, Y. TOMMII and H. MAZAKI, *Jpn J. Appl. Phys.* **27** (1988) L1041.
9. U. ENDO, S. KOYAMA and T. KAWAI, *ibid.* **27** (1988) L1476.
10. B. W. STATT, Z. WANG, M. J. G. LEE, J. V. YAKHMI and P. C. DECAMARGO, *Physica C* **156** (1988) 251.
11. C. T. CHU and B. DUNN, *J. Amer. Ceram. Soc.* **70** (1987) 375.
12. R. SANJINES, K. R. THAMPI and J. KIWI, *ibid.* **71** (1988) L512.

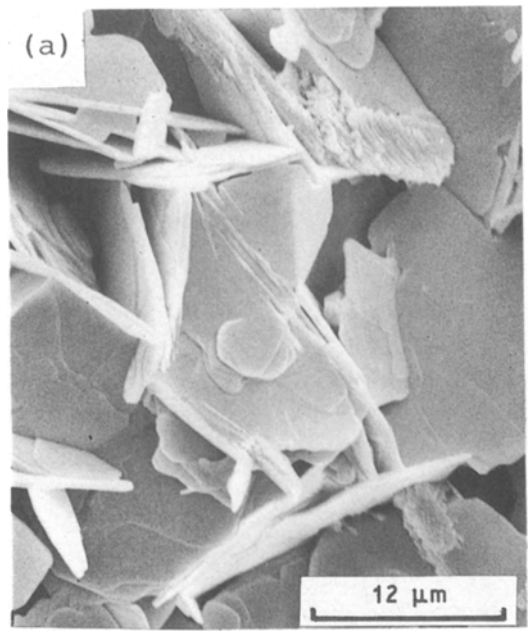

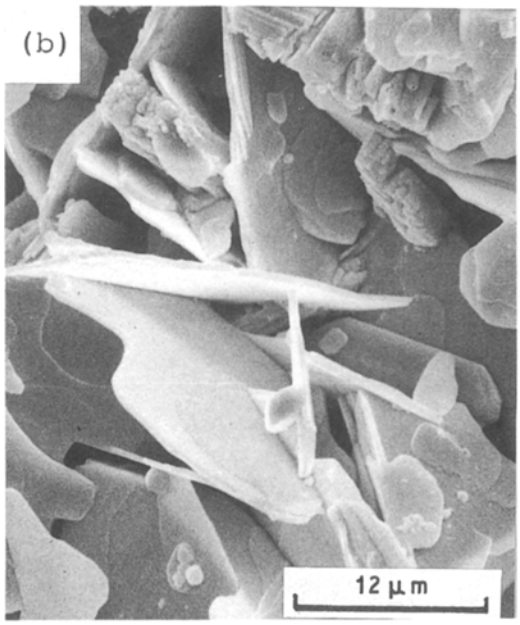

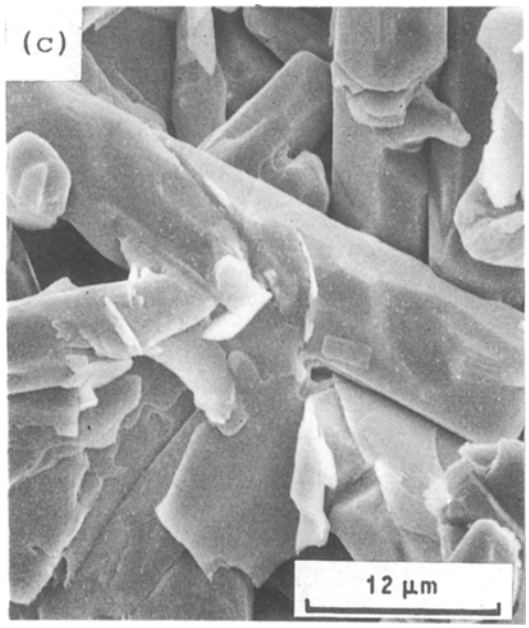

Figure 7 Scanning electron micrographs of $Bi_{0.8}Pb_{0.2}SrCaCu_2O_y$ sintered at 840° C for (a) 5 h, (b) 16 h and (c) 40 h.

13. P. BARBONX, J. M. TARASCON, L. H. GREENE, G. W. HULL and B. G. BAGLEY, *J. Appl. Phys.* **63** (1988) 2725.
14. F. H. CHEN, H. S. KOO, T. Y. TSENG, R. S. LIU and P. T. WU, *Mater. Lett.* **8** (1989) 228.
15. F. R. SALE and F. MAHLOOJCHI, *Ceram. Int.* **14** (1988) 229.
16. C. J. BRINKER and G. W. SCHERER, in "Ultrastructure Processing of Ceramics, Glasses, and Composites", edited by L. L. Hench and D. R. Ulrich (Wiley, New York, 1984) pp. 43–59.
17. T. Y. TSENG, C. C. LIN and J. T. LIAW, *J. Mater. Sci.* **22** (1987) 965.
18. C. MICHEL, M. HERVIEN, H. M. BOREL, A. GRANDIN, F. DESLANDES, J. PROVOST and B. RAVEAU, *Z. Phys. B* **68** (1987) 421.
19. J. AKIMITSU, A. YAMAZAKI, H. SAWA and H. FUJIKI, *Jpn J. Appl. Phys.* **27** (1987) L209.
20. N. KIJIMA, H. ENDO, J. TSUCHIYA, A. SUMIYAMA, M. MIZUNO and Y. OGURI, *ibid.* **28** (1988) L1852.
21. T. UZUMAKI, K. YAMANAKA, N. KAMEHARA and K. NIWA, *ibid.* **28** (1989) L75.
22. U. KUXMANN and F. FISCHER, *Erzmetall* **27** (1974) 533.
23. Z. Y. RAN, X. CHU, J. H. WANG, D. N. ZHENG, S. L. JIA, Z. H. MAI and Z. X. ZHAO, *Mod. Phys. Lett.* **B2** (1988) 699.
24. P. V. P. S. S. SASTRY, I. K. GOPALAKRISHNAN, J. V. YAKHMI and R. M. IYER, *Physica C* **157** (1988) 491.
25. W. HERKERT, H. W. NEUMUELLER and M. WILHELM, *Solid State Commun.* **69** (1989) 183.

Received 4 May
and accepted 13 September 1989